Supporting information for

Integrated Passivation Strategy Using Multifunctional Additives for Tin-Lead Mixed Perovskite Solar Cells

Dong He[1,2], Gongcheng Zhou[2,3], Zeyu Niu[2], Guoqiang Guo[2], Tianle Cheng[2], Gangsen Su[2], Haojie Chen[2], Siyuan Tang[2], Jiacheng He[2], Wenhua Zhang,[3] Zhubing He[2,] *

[1] School of Materials Science and Engineering, Harbin Institute of Technology, Harbin 150001 China.

[2] Department of Materials Science and Engineering, Shenzhen Key Laboratory of Full Spectral Solar Electricity Generation (FSSEG), Southern University of Science and Technology (SUSTech), No. 1088, Xueyuan Rd, Shenzhen, 518055, Guangdong, China.

[3] School of Materials and Energy, Yunnan University, Kunming, 650091, Yunnan, China

*Corresponding author. Email: hezb@sustech.edu.cn

Experimental

Materials and Methods

Materials

Anhydrous solvents, including N, N-dimethylformamide (DMF), dimethyl sulfoxide (DMSO), chlorobenzene (CB), and isopropanol (IPA), were obtained from Sigma-Aldrich. Lead iodide (PbI_2, 99.99%) and ethylenediamine dihydroiodide ($EDAI_2$, 99.99%) were sourced from TCI. Formamidinium iodide (FAI, 99.99%) and methylammonium iodide (MAI, 99.99%) were acquired from Great Cell Solar. Bathocuproine (BCP, >99%), phenyl-C_{61}-butyric acid methyl ester ($PC_{61}BM$, >99%), and PEDOT:PSS were purchased from Xi'an Yuri Solar Co., Ltd. N-(4-Cyanophenyl) guanidine hydrochloride (CG) was obtained from Bide Pharmatech Ltd. Silver (Ag) and tin fluoride (SnF_2) were sourced from Sigma-Aldrich, while tin iodide (SnI_2) was provided by Energy Chemical. Fullerene (C60) was purchased from Liaoning Youxuan New Energy Technology Co., Ltd. Methyl sulfoxide-d6 was obtained from J&K Scientific, and ITO glass from Suzhou ShangYang Solar Technology Co., Ltd.

To prepare the undoped precursor solution, 14.2 mg of SnF_2, 85.8 mg of MAI, 216.6 mg of FAI, 415 mg of PbI_2, and 335.6 mg of SnI_2 were dissolved in 1000 μL of a DMF and DMSO mixture (volume ratio 7:3). The solution was stirred for 12 hours. For the doped solution, an additional 1.6-2.4 mg of CG was added to the undoped precursor solution.

To prepare the passivation solution, 5 mg of $EDAI_2$ was dissolved in 10 mL of a 200:1 volume ratio of IPA and DMF. For the integrated passivation solution, an additional 1-3 mg of CG was added to the blank passivation solution. The solution was stirred for 24 hours.

Device fabrication

The inverted (p-i-n) perovskite solar cell examined in this study features an architecture of ITO/PEDOT:PSS/Perovskite/$EDAI_2$/$PC_{61}BM$/C60/BCP/Ag. The fabrication process began with cleaning the ITO glass substrate in an ultrasonic bath, sequentially using detergent (2% in deionized water), deionized water, acetone, and isopropanol, each for 15 minutes. The cleaned substrate was then dried with N_2 gas and subjected to

UV-ozone treatment for 15 minutes. The PEDOT:PSS dispersion was spin-coated onto the ITO substrate and annealed at 150℃ for 10 minutes. After transferring the substrates to a glovebox, the prepared perovskite precursor solution was spin-coated onto the PEDOT:PSS layer, initially at 1000 rpm for 10 seconds, then at 5000 rpm for 60 seconds. During the final 25 seconds, 500 μL of chlorobenzene was drop-cast onto the spinning film, which was then annealed at 100℃ for 10 minutes. A solution mix of CG and $EDAI_2$ was dynamically spin-coated onto the perovskite layer at 4000 rpm for 35 seconds, followed by annealing at 100℃ for 5 minutes. A layer of $PC_{61}BM$ (3 mg/mL in chlorobenzene) was then spin-coated at 6000 rpm for 35 seconds and annealed at 100℃ for 30 seconds. This was followed by the thermal evaporation of a 20 nm layer of C60 and a 6 nm layer of BCP. Finally, a 100 nm thick layer of silver (Ag) was deposited via thermal evaporation to complete the device structure.

Materials characterizations:

The NMR spectra were recorded using Bruker Advance 500 and Bruker Advance 400 spectrometers in DMSO-d6. UV-Vis spectra were obtained on a PerkinElmer Lambda 950 spectrometer. Steady-state and time-resolved PL spectra were measured with a Photoluminescence Spectrometer (FLS1000, Edinburgh Instruments) using a 532 nm pulsed laser as the excitation source. For film characterization, X-ray diffraction (XRD) spectra were measured with a Rigaku Smartlab. The XRD results were obtained using a focused-beam setup. Subsequently, grazing-incidence XRD (GIXRD) measurements were performed with a parallel-beam geometry, which is optimized for thin-film characterization. Additionally, prior to testing each sample, parallel-beam alignment was conducted to ensure accurate sample height calibration. The samples were then tested at incident angles of 0.3°, 0.5°, 1.0°, and 3.0°. X-ray photoelectron spectroscopy (XPS) measurements were performed on an Omicron ESCA Probe XPS spectrometer (Thermo Scientific ESCALAB 250Xi) with a survey scan pass energy of 150 eV and step size of 1 eV, and a fine scan pass energy of 20 eV with a 0.01 eV step size. Scanning electron microscopy (SEM) images were obtained using a HITACHI SU8230. FTIR spectra were recorded on a Bruker Vertex 70v. Ultraviolet photoelectron spectroscopy

(UPS) spectra, used to measure the work function, were recorded on an Imaging Photoelectron Spectrometer (Axis Ultra, Kratos Analytical Ltd) with a non-monochromated He Iα photon source (hν = 21.22 eV), using Au as a reference.

Device performance characterization:

J-V measurements were performed using a Keithley 2400 source meter in ambient conditions (~20 °C and ~60% RH). Unencapsulated devices were tested in both reverse scan (0.9 V to -0.2 V, with 0.01 V steps) and forward scan (-0.2 V to 0.9 V, with 0.01 V steps), with a delay of 200 ms. Illumination was provided by an Oriel Sol3A solar simulator with an AM 1.5G spectrum, calibrated to a light intensity of 100 mW/cm^2 using a standard KG-5 silicon diode. A shadow mask defined the active area (0.08 cm^2) during measurements. Electrochemical impedance spectroscopy (EIS) and Mott-Schottky plots were obtained using a Zahner Zennium electrochemical workstation. EQE measurements were conducted with an EnliTech (Taiwan) system, with light intensity at each wavelength calibrated using a standard single-crystal silicon photovoltaic cell. For stabilized power output (SPO) tests under illumination, the bias voltage was held at the maximum power point voltage (*Vmax*), and current density was monitored under ambient conditions without temperature control. Long-term operational stability was evaluated by placing encapsulated devices under a 1 sun equivalent LED lamp in ambient conditions (~20 °C and ~60% RH), with maximum power point data recorded every minute.

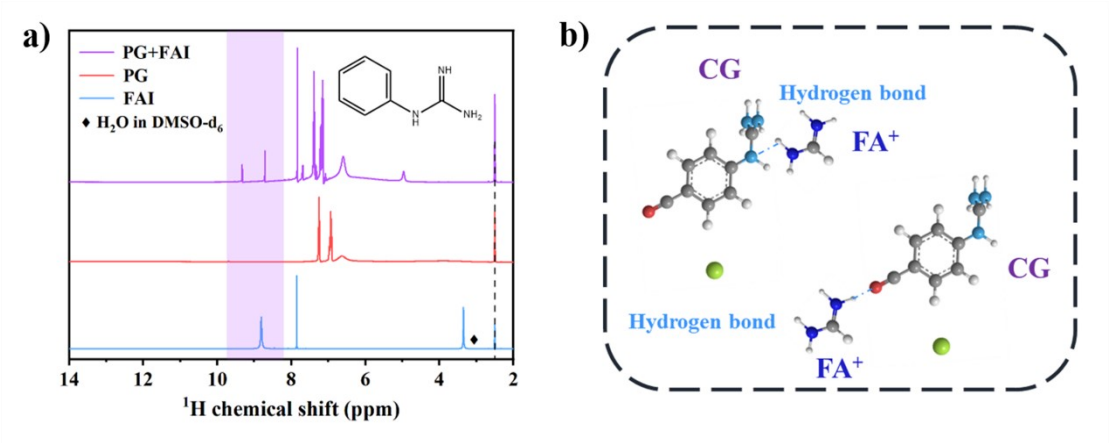

Figure S1. a) ^{1}H nuclear magnetic resonance (NMR) spectroscopy of phenylmethylguanidine (PG), FAI and PG+FAI. b) Schematic diagram of hydrogen bonding between FA^{+} and CG.

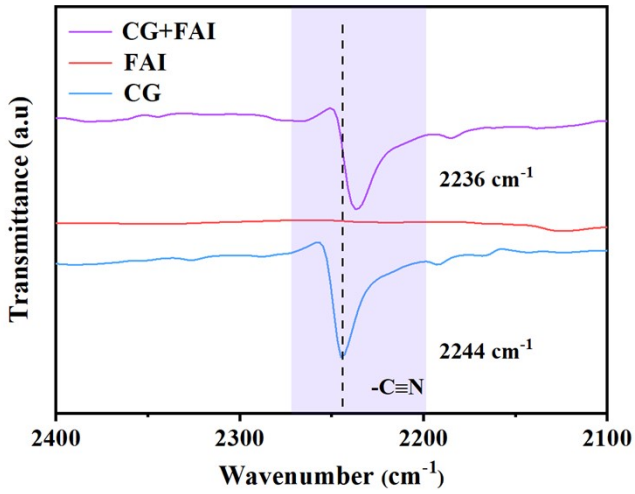

Figure S2. FTIR spectrum of CG, FAI and CG+FAI.

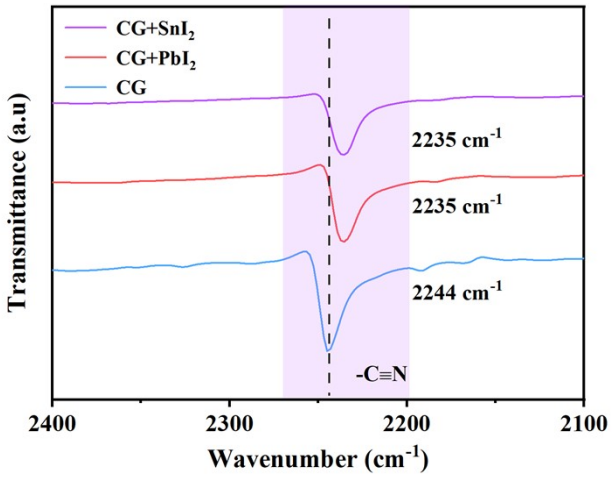

Figure S3. FTIR spectrum of CG, CG+PbI_2 and CG+SnI_2.

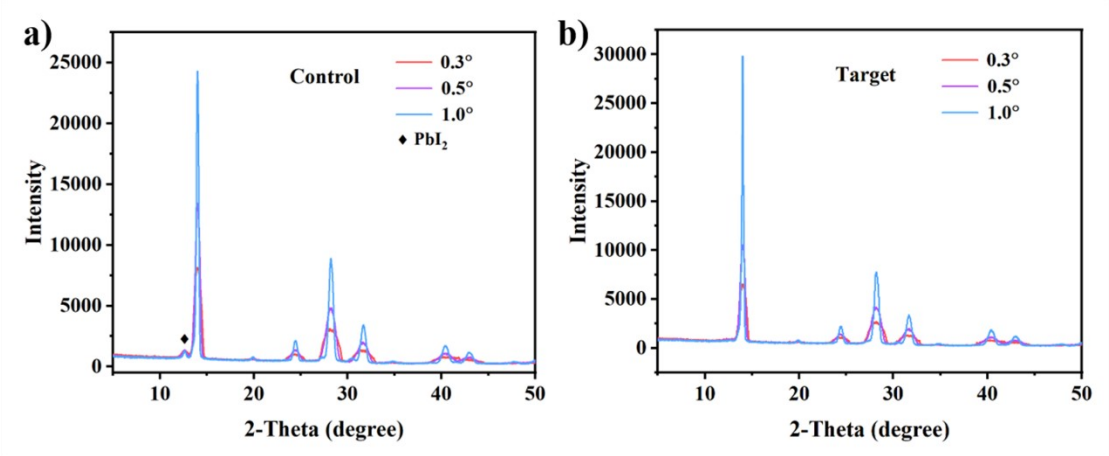

Figure S4. The grazing incidence X-ray diffraction (GIXRD) patterns of a) Control and b) target TLP films.

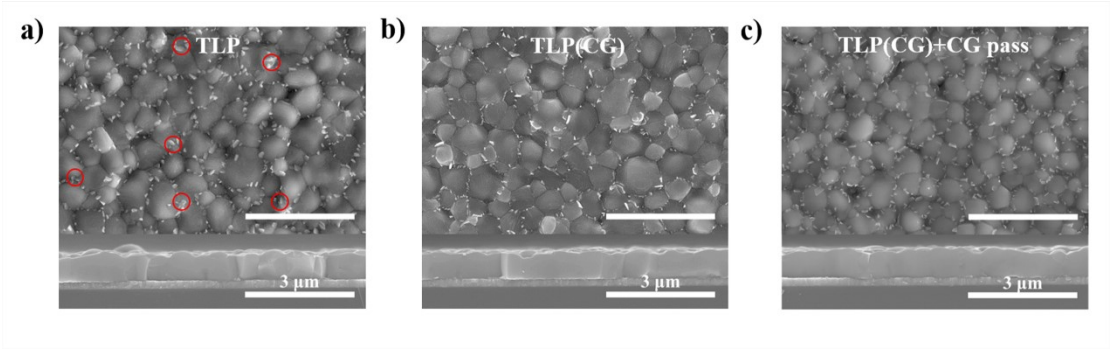

Figure S5. The top-view and cross-section scanning electron microscope (SEM) images of TLP-control a), b) TLP(CG) and c) TLP(CG)+CG pass-target.

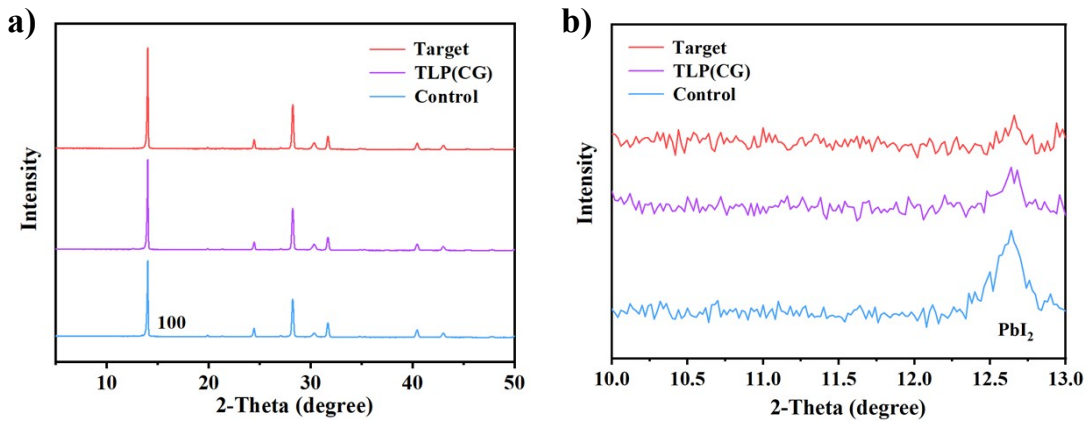

Figure S6. The grazing incidence X-ray diffraction (GIXRD) patterns of TLP-control, TLP(CG) and TLP(CG)+CG pass-target films.

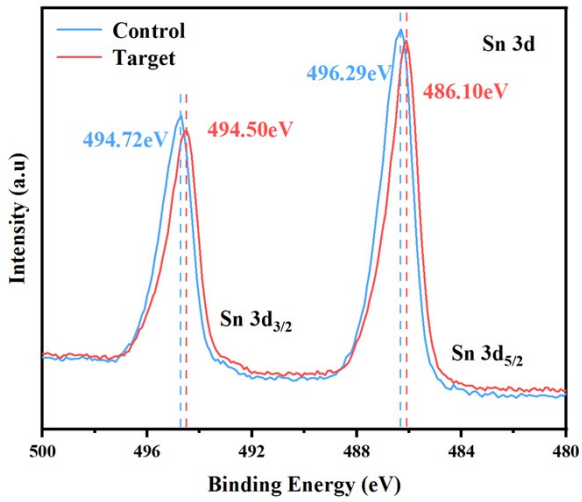

Figure S7. The XPS peaks of Sn 3*d* for control and target TLP films.

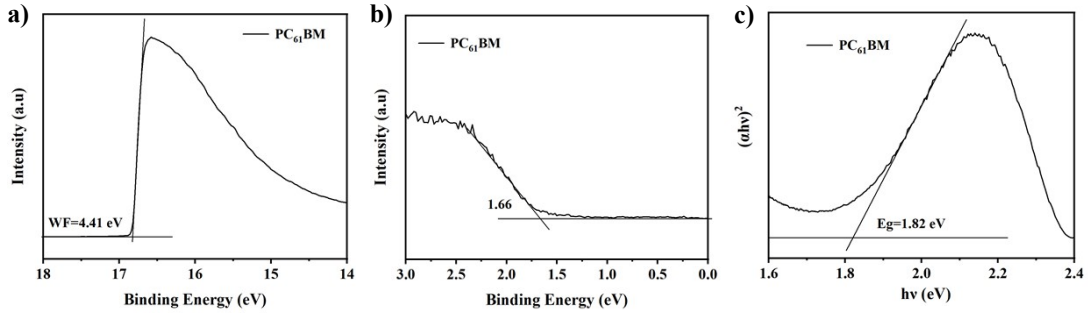

Figure S8. Ultraviolet photoelectron spectroscopy (UPS) spectra of $PC_{61}BM$ film a) and b). c) Tauc plot of $PC_{61}BM$ film.

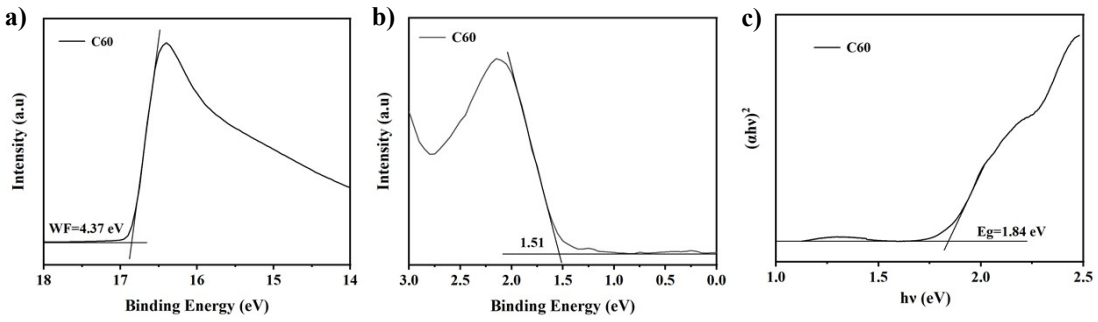

Figure S9. Ultraviolet photoelectron spectroscopy (UPS) spectra of C60 film a) and b). c) Tauc plot of C60 film.

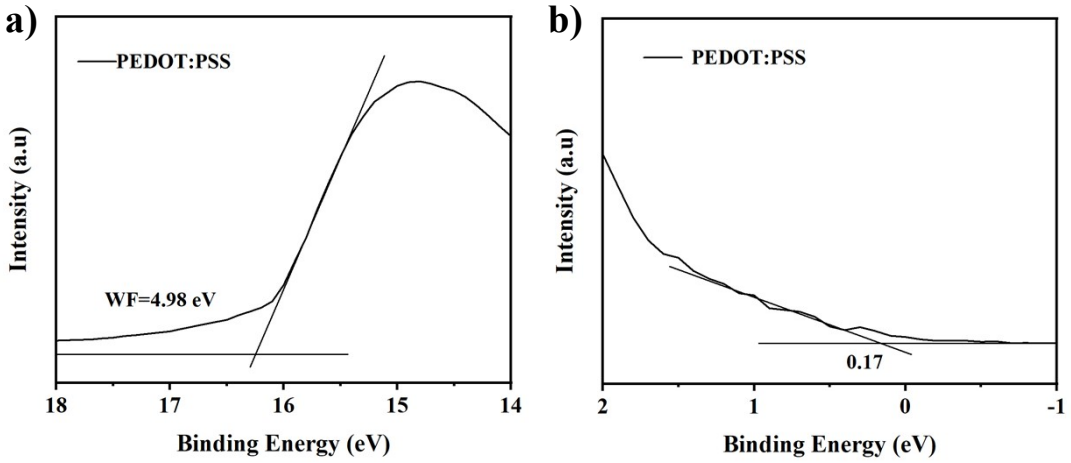

Figure S10. Ultraviolet photoelectron spectroscopy (UPS) spectra of PEDOT:PSS film a) and b).

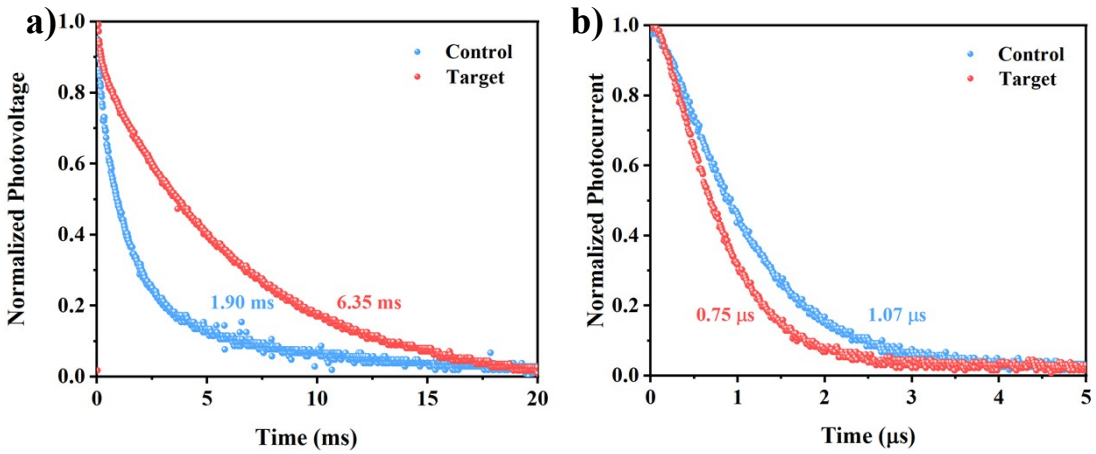

Figure S11. Transient photovoltage (TPV) and transient photocurrent (TPC) tests of control and target devices.

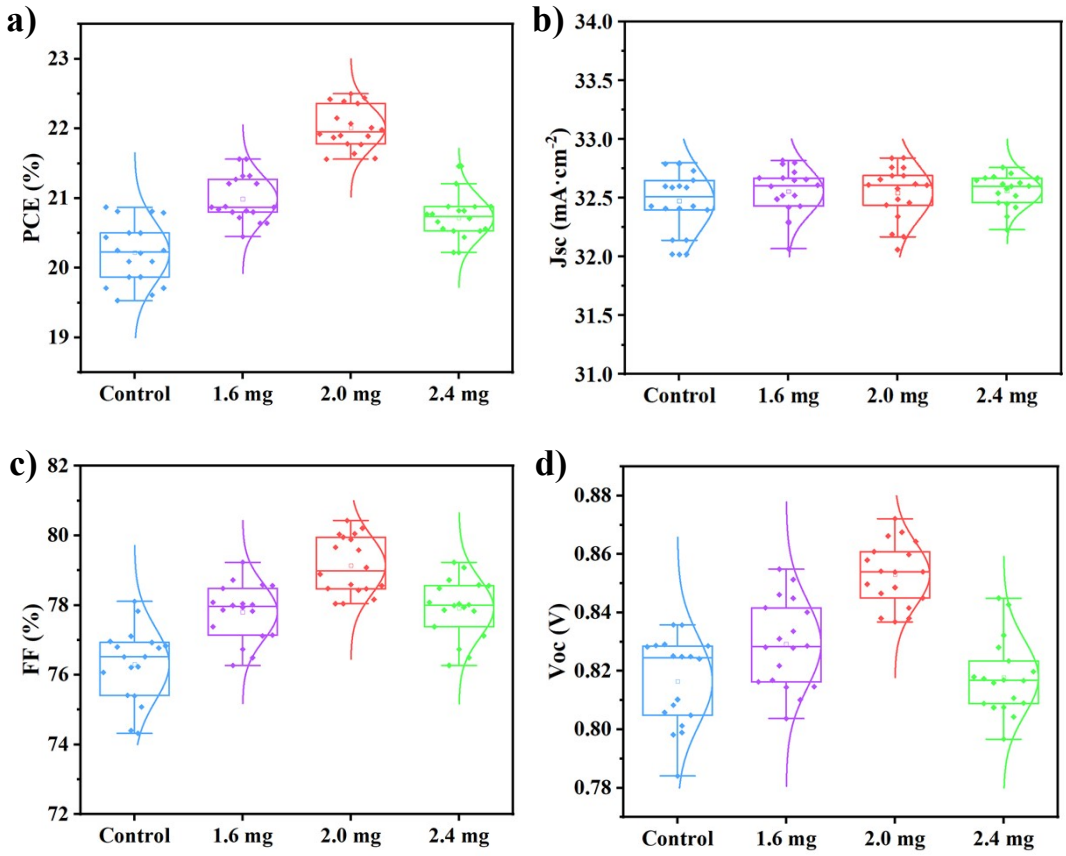

Figure S12. Distribution of performance parameters of PSCs conversion efficiency after CG incorporation.

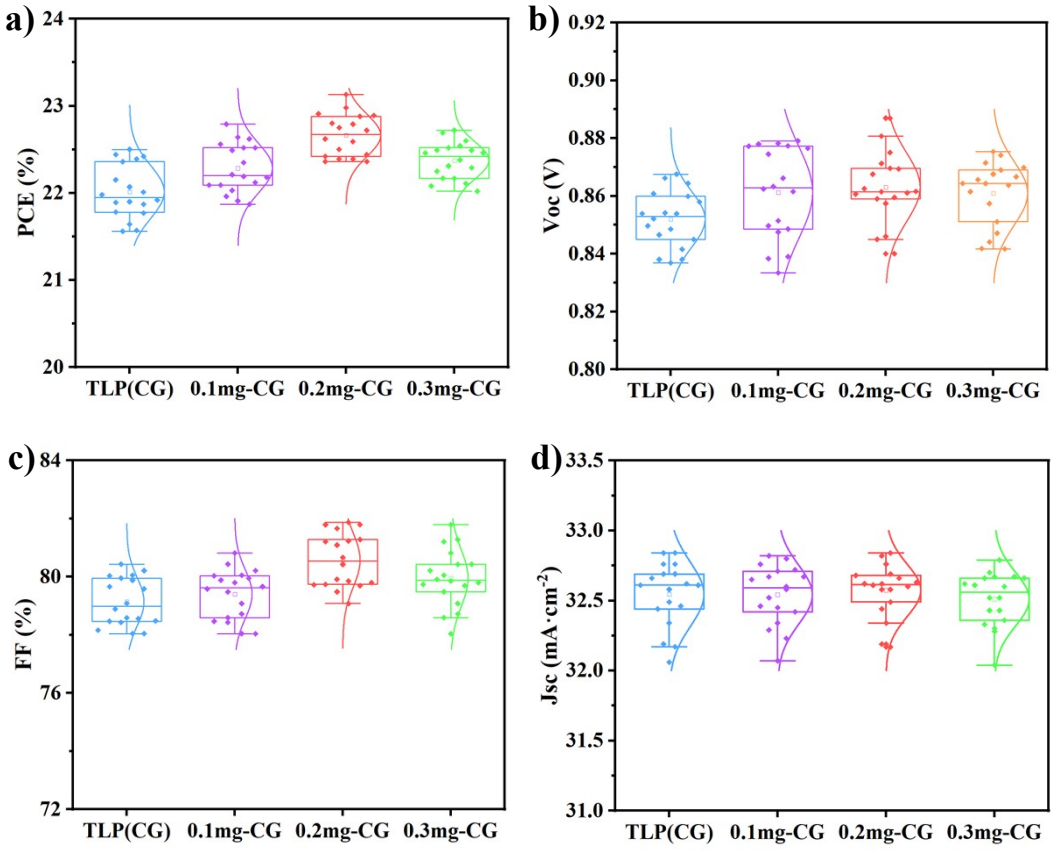

Figure S13. Distribution of performance parameters of PSCs conversion efficiency after CG incorporation and CG passivation.

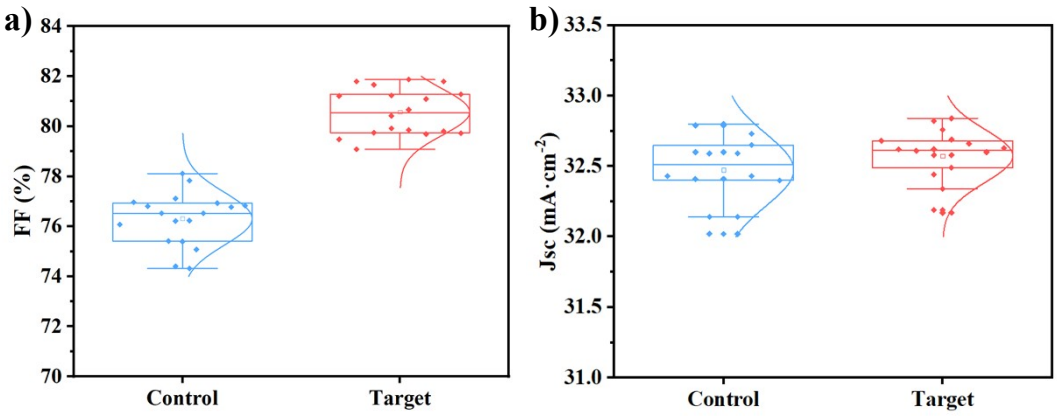

Figure S14. Distribution of performance parameters of PSCs conversion efficiency without and with CG incorporation and CG passivation.

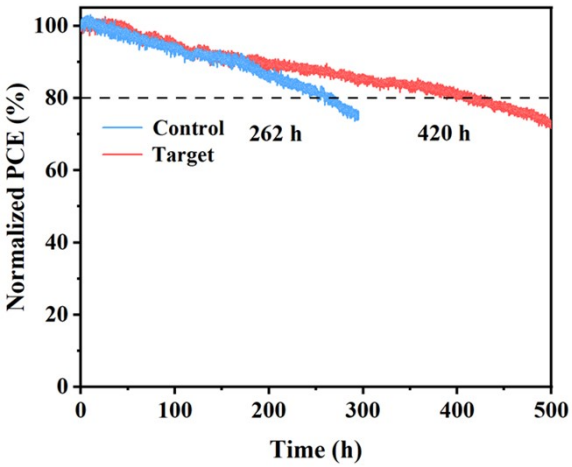

Figure S15. Encapsulated PSCs with maximum output point continuous tracking under AM1.5G illumination in ambient air.

Table S1. The fitting results of TRPL for Control and Target perovskite films.

	A_1	τ_1 (ns)	A_2	τ_2 (ns)	R^2	τ_{ave} (ns)
Control	**0.6430**	**830**	**0.3570**	**4800**	**0.9983**	**2247**
Target	**0.5468**	**895**	**0.4532**	**8772**	**0.9991**	**4464**

Table S2. The detail data of the *JV* curves of PSCs with CG incorporation.

	J_{SC} (mA/cm^2)	V_{OC} (V)	*FF* (%)	PCE (%)
Control	**32.59**	**0.840**	**76.02**	**20.81**
1.6mg/mL	**32.60**	**0.842**	**78.58**	**21.56**
2.0mg/mL	**32.73**	**0.853**	**80.59**	**22.50**
2.4mg/mL	**32.63**	**0.842**	**78.04**	**21.44**

Table S3. The detail data of the *JV* curves of PSCs with CG incorporation and passivation.

	J_{SC} (mA/cm^2)	V_{OC} (V)	*FF* (%)	PCE (%)
TLP(CG)	**32.73**	**0.853**	**80.59**	**22.50**
0.1mg/mL	**32.76**	**0.862**	**80.17**	**22.64**
0.2mg/mL	**32.84**	**0.860**	**81.87**	**23.13**
0.3 mg/mL	**32.79**	**0.848**	**81.79**	**22.74**

Table S4. The detail data of the *JV* curves of PSCs.

		J_{SC} (mA/cm^2)	V_{OC} (V)	*FF* (%)	PCE (%)
Control	**Forward**	**32.59**	**0.840**	**76.02**	**20.81**
	Reverse	**32.40**	**0.829**	**73.38**	**19.71**
Target	**Forward**	**32.84**	**0.860**	**81.87**	**23.13**
	Reverse	**32.62**	**0.859**	**80.01**	**22.42**

Table S5. Fitting parameters of PSCs from Nyquist plots.

	R_S (Ω)	R_{REC} (Ω)
Control	**44.7**	**1559**
Target	**41.9**	**4738**